On the diffusion current in a MOSFET operated down to deep cryogenic temperatures

G. Ghibaudo, M. Aouad, M. Casse, T. Poiroux, Christoforos Theodorou

Solid State Electronics, in press (2021)

On the diffusion current in a MOSFET operated down to deep cryogenic temperatures

G. Ghibaudo[1], M. Aouad[2], M. Casse[2], T. Poiroux[2], C. Theodorou[1],

1) IMEP-LAHC, Université Grenoble Alpes, MINATEC/INPG, 38016, Grenoble (France)
2) Université Grenoble Alpes, CEA, Leti, F-38000 Grenoble (France)
Email: gerard.ghibaudo@grenoble-inp.fr

Abstract

A detailed and didactic analysis of the diffusivity in a 2D inversion layer is carried out, providing its dependence on carrier density and temperature. Then, a comprehensive study of the diffusion and drift current components in a MOSFET is proposed. Their dependence with gate and drain voltages is investigated down to deep cryogenic temperature, revealing that at T=4K the diffusion current is nearly constant in strong inversion whatever the mobility law. Finally, based on our diffusivity analysis, a new formulation of the diffusion noise valid from weak to strong inversion down to very low temperature has been developed.

Keywords: MOSFET, diffusion current, diffusion noise, cryogenic temperature.

1. Introduction

The MOSFET is a crucial component in the microelectronics era [1,2]. Due to its high performance in terms of on-current and turn-on behaviour, it has valuably been employed in CMOS technologies e.g. for digital applications. Recently, a regain of interest for cryogenic electronics has emerged for use in readout CMOS circuits for quantum computing application [3-5]. In this respect, a clear understanding of the MOSFET operation is still a key issue, especially in subthreshold region where carrier diffusion dominates and above threshold where drift prevails [1,2]. At deep cryogenic temperature, however, the subthreshold slope greatly increases, reducing in turn the subthreshold voltage range. Hence, the question about the diffusion current component arises since the carrier diffusivity D should decrease according to the Einstein relation, qD=μ.kT, at least for a constant mobility. Besides, the carrier diffusion has an important contribution to the white noise in MOSFET and should be addressed [6-8].

Therefore, in this work, we propose a comprehensive analysis of the MOSFET diffusion current from subthreshold to above threshold region both in linear and saturation regimes and down to deep cryogenic temperatures. To this end, we first review in a didactic way the definitions of the carrier diffusivity depending on the carrier statistics i.e. Boltzmann, Fermi-Dirac and degenerate metallic ones. Then, using a template MOS device with a single 2D subband, we analyse in an original way the diffusion current component in all operation regimes and versus temperature down 4K range. Finally, we revisit the formulation of the diffusion noise in a MOSFET down to deep cryogenic temperatures.

2. Carrier diffusivity in MOSFET inversion layer

By stating that, at equilibrium, the electrochemical potential gradient is zero along the transport coordinate x, or in other words that the drift current, J_{drift}=q.n.μ.dψ/dx, is compensated by the diffusion current, J_{diff}=-q.D.dn/dx, where q is the magnitude of the electron charge, n is the carrier density, μ the carrier mobility in the channel and ψ the electrical potential in the channel, it is easy to show that, in the most general case, the carrier diffusivity D is given by the generalized Einstein relation [9],

$$q.D = \mu.n.\frac{\partial Ef}{\partial n}, \quad \text{(Fermi-Dirac statistics)} \tag{1}$$

E_f being the Fermi level.

In the case of Boltzmann statistics, since $\partial n/\partial E_f = n/kT$, it reduces to the usual Einstein relation:

$$q.D = \mu.kT, \quad \text{(Boltzmann statistics)} \tag{2}$$

k being the Boltzmann constant and T the temperature.

In the case of metallic statistics (full degeneracy), and considering for the sake of simplicity, that the MOSFET inversion layer is depicted by a single 2D subband of density of states A_{2d}, which is realistic at low temperature, we have $n=A_{2d}.E_f$, such that the carrier diffusivity takes the form [10],

$$q.D = \mu.E_f. \qquad \text{(Metallic statistics)} \tag{3}$$

The carrier density in a single 2D subband is given by [11,12],

$$n = kT.A_{2d}.ln\left(1 + e^{Ef/kT}\right), \tag{4}$$

where the 2D density of states is given by $A_{2D}=g.m_d^*/(\pi.\hbar)$ with g the subband degeneracy factor, m_d^* the DOS effective mass and $\hbar$ the reduced Planck constant.

Using Eq. (4), it is easy to show that the diffusivity of Eq. (1) can be related to the carrier inversion layer density by,

$$q.D = \mu.\frac{n}{A_{2d}}.\frac{e^{\frac{n}{kT.A_{2d}}}}{\left(e^{\frac{n}{kT.A_{2d}}}-1\right)}, \tag{5}$$

which can also be equated to in terms of inversion layer charge Q_i (absolute value) and quantum capacitance, $C_q=q.A_{2d}$, as,

$$D = \mu.\frac{Q_i}{C_q}.\frac{e^{\frac{q.Q_i}{kT.C_q}}}{\left(e^{\frac{q.Q_i}{kT.C_q}}-1\right)}. \tag{6}$$

Figure 1 illustrates the variation of the diffusivity with temperature in log or linear scale as obtained using Eq. (6) for various inversion layer charges with a constant mobility μ=1000 cm^2/Vs. As can be seen, the carrier diffusivity D shows mostly a linear dependence with temperature, in accordance with Einstein's relation, except at low temperature where it is saturating to a constant value given by Eq. (3) and which depends on inversion layer charge. It should be noted that, in the most general case, these variations of D with temperature should also account for the mobility dependence with temperature. Nevertheless, it is worth emphasizing that, from Fig. 1, the carrier diffusivity at very low temperature is saturating to a value governed by the metallic statistics and that the classical Einstein relation is useless.

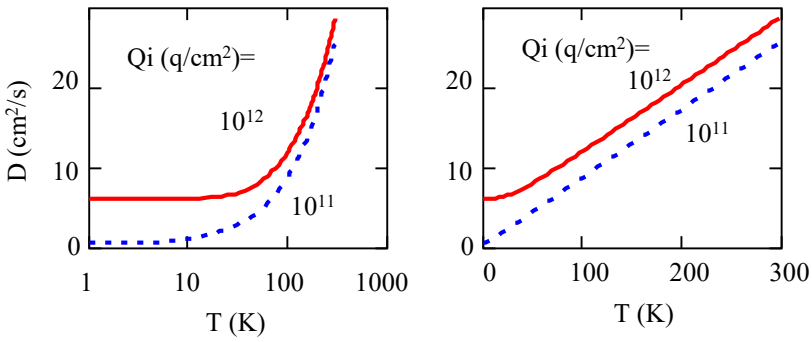

Fig. 1. Variation of carrier diffusivity D with temperature for two inversion layer charges in log (left) or linear (right) scale (μ= 1000 cm^2/Vs).

Another interesting situation at cryogenic temperatures considers the presence of an exponential band tail below the subband edge [13-15]. In this case, the energy density of states N(E,ΔE) with an exponential band tail can be described by [16],

$$N(E,T_0) = \frac{A_{2d}}{1+\exp(-\frac{E}{kT_0})}, \tag{7}$$

where T_0 is a characteristic temperature in the range 30-50K [14-16]. For degenerate (metallic) statistics, i.e. when $T<<T_0$, integration of Eq. (7) over energy between -∞ to E_f yields for the 2D carrier inversion layer density,

$$n(E_f,T_0) = kT_0.A_{2d}.ln\left[1+exp\left(\frac{E_f}{k.T_0}\right)\right]. \tag{8}$$

As a result, it is worth noting that, in this case, the 2D carrier density is given by the same expression as in Eq. (4) for a single subband without band tail but with the temperature T_0, regardless of the real temperature, provided $T<<T_0$.

The corresponding diffusivity can now be evaluated using Eq. (1), yielding,

$$D(E_f,T_0) = \mu.kT_0.\ln\left[1+exp\left(\frac{E_f}{kT_0}\right)\right].\left[1+exp\left(-\frac{E_f}{kT_0}\right)\right]. \tag{9}$$

Figure 2a shows the variation of diffusivity given by Eq. (9) with the Fermi level E_f for a constant mobility. One can see that, for E_f well above the band edge i.e. $E_f>>0$, the diffusivity varies linearly with the Fermi level in accordance with the metallic statistics limit of Eq. (3), which is undefined for $E_f<0$. In contrast, for E_f well below the band edge i.e. $E_f<<0$, the diffusivity saturates to the value $D=\mu.kT_0/q$ as in Eq. (2), but now with T_0 playing the role of the temperature. Figure 2b&c shows the corresponding variations of diffusivity with carrier inversion layer in linear and log scale. Similarly, the diffusivity varies linearly with n for $n>>kT_0.A_{2d}$ (≈$5.10^{11}/cm^2$) well above band edge, whereas the diffusivity saturates to $\mu.kT_0/q$ for $n<<kT_0.A_{2d}$.

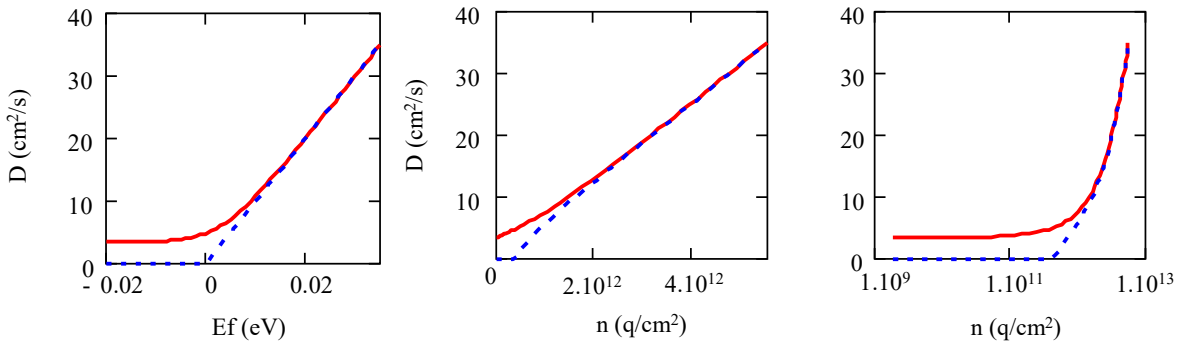

(a) (b) (c)

Fig. 2. Variations of carrier diffusivity D with a) Fermi level E_f, b) and c) carrier inversion layer density n in linear and log scale for a 2D single subband with a band tail with T_0=40K. Solid lines: Eq. (9), dashed lines: metallic statistics limit of Eq. (3) (Constant mobility μ= 1000 cm^2/Vs).

In the above discussion, we assumed, for simplicity, a constant mobility for the calculation of the diffusivity. One might wonder whether this assumption is not too simplistic as compared to experiment. To this end, we have derived using Eq. (5) the experimental diffusivity from typical experimental effective mobility data $\mu_{eff}(n)$ obtained by split C-V technique on 28nm FDSOI MOSFETs (see Fig. 3a). As is usual at very low temperature [17], the effective mobility displays a bell-shaped behavior at T=4.2K, whereas it decreases in amplitude and flattens up at strong inversion for T=200K. As can be seen from Fig. 3b, even though μ_{eff} is not constant versus 2D carrier density, the overall variation of the associated diffusivity D with 2D carrier density exhibits a linear trend (blue dashed line), well fitted by the metallic statistics limit of Eq.(3) with a constant mobility.

This feature justifies why we will still assume, in first instance, a constant mobility in the following sections for the MOSFET modelling and subsequent discussion of the results about diffusion partition in device operation.

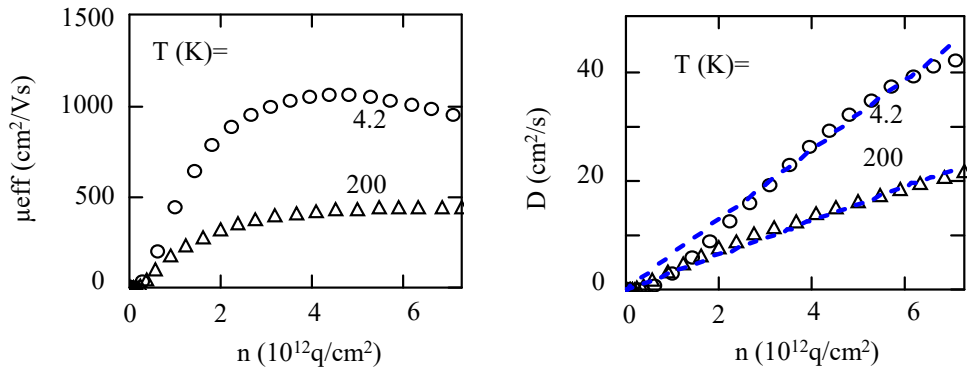

(a) (b)

Fig. 3. a) Experimental (symbols) variation of effective mobility μ_{eff} with 2D carrier density n at T=4.2K and T=200K. Typical μ_{eff} experimental data from 10µm×10µm 28nm FDSOI MOSFET with 1.8nm EOT gate oxide, 7nm silicon and 30nm bottom oxide. b) Corresponding experimental (symbols) variation of diffusivity D with 2D carrier density n at T=4.2K and T=200K. The diffusivity D is calculated using Eq. (5). The blue dashed lines show the linear trends obtained for a constant mobility (Resp. µ= 1080 and 500 cm^2/Vs) using the metallic statistics limit of Eq. (3).

2. MOSFET diffusion current modelling

In the gradual channel approximation, the drain current in a long channel MOSFET $I_d=W.\mu.Q_i.dU_c/dx$, is obtained after integration along the channel coordinate x as [1,2],

$$I_d = \frac{W}{L}\int_0^{V_d} \mu.\, Q_i(\psi_s - U_c)dU_c \tag{10}$$

where ψ_s is the surface potential, U_c the quasi-Fermi level shift between source (@0V) and drain (@V_d), V_d the drain voltage and W and L the channel width and length, respectively.

Similarly, the diffusion current component, $I_{ddiff}=-W.D.dQ_i/dx$, can be obtained in the form,

$$I_{ddiff} = -\frac{W}{L}\int_{Q_{is}}^{Q_{id}} D(Q_i)dQ_i \tag{11}$$

where Q_{is} and Q_{id} are the inversion layer charge at source and drain end, respectively. The diffusion current could be further evaluated using Eq. (11) after specifying D(Qi) as given by Eq. (6) for a subband without band tail or Eq. (11) for a degenerate subband with band tail. In any case, the drift current component I_{ddrift} can in turn be evaluated after subtracting the diffusion current as $I_{ddrift}=I_d-I_{ddiff}$.

It is interesting to formulate the diffusion current in the two limiting cases *i.e.* Boltzmann and degenerate metallic statistics where the diffusivity takes a simple form. In fact, using Eqs (2), (3) and (11) yields, assuming a constant mobility, for the diffusion current:

$$I_{ddiff} = \frac{W}{L}.\frac{kT}{q}.\mu.(Q_{is} - Q_{id}) \qquad \text{(Boltzmann statistics)} \tag{12a}$$

$$I_{ddiff} = \frac{W}{2L}.\frac{\mu}{C_q}.(Q_{is}^2 - Q_{id}^2). \qquad \text{(Metallic statistics)} \tag{12b}$$

To go further and compute the drain current in the device, we have to define a MOSFET structure. To this end, we choose for template device a FDSOI MOSFET having an equivalent gate oxide thickness t_{ox}=2nm, a silicon film thickness t_{si}=10nm and a bottom oxide thickness t_{box}=30nm. These values are typical for a 28nm FDSOI CMOS technology [18]. For this structure, the gate charge conservation equation for the front channel reads [16,19],

$$V_g = V_{fb} + \psi_s + \frac{Q_i(\psi_s - V_0 - U_c)}{C_{ox}} + \frac{C_b.(\psi_s - V_b)}{C_{ox}} \tag{13}$$

where V_{fb} is the flat band voltage, $V_0=E_g/2q$ for an undoped silicon film (E_g being the silicon bandgap), V_b is the bottom gate bias, C_{ox} is the gate oxide capacitance ($=\varepsilon_{ox}/t_{ox}$), $C_b=C_{si}.C_{box}/(C_{si}+C_{box})$ is the back gate coupling capacitance with C_{si} being the Si film capacitance ($=\varepsilon_{si}/t_{si}$) and C_{box} the bottom oxide capacitance ($=\varepsilon_{ox}/t_{box}$).

It is worth mentioning that an alternative derivation of the drift and diffusion current components can be formulated using Eqs (10) and (13). As a matter of fact, it can be noticed that the variations of ψ_s along the channel are related to the drift electric potential gradient, whereas the variations of (U_c-ψ_s) along x are linked to the diffusion potential gradient. As a result, it is easy to show using Eq. (13) that $d\psi_s=C_{inv}/(C_{inv}+C_{ox}).dU_c$, such that the drain components can be expressed as,

$$I_{ddrift} = \frac{W}{L}\int_0^{V_d} \mu.\, Q_i(\psi_s - U_c).\, dV_s = \frac{W}{L}\int_0^{V_d} \mu.\, Q_i(\psi_s - U_c).\frac{C_{inv}}{C_{inv}+C_{ox}}\, dU_c, \quad (14a)$$

$$I_{d,diff} = \frac{W}{L}\int_0^{V_d} \mu.\, Q_i(\psi_s - U_c).\, (dU_c - d\psi_s) = \frac{W}{L}\int_0^{V_d} \mu.\, Q_i(\psi_s - U_c).\frac{C_{ox}}{C_{inv}+C_{ox}}\, dU_c, \quad (14b)$$

where the inversion charge capacitance is given by $C_{inv}=\partial Q_i/\partial\psi_s$. Of course, one can easily see that adding I_{ddiff} and I_{ddrift} allows recovering I_d. Moreover, it can be shown using the generalized Einstein relation of Eq. (1) that this formulation is perfectly equivalent to the diffusion approach of Eq. (11). It also means that the diffusion and drift drain current components can be evaluated using Eqs (14) without using the diffusivity relations.

To close this section, we would like to examine the consequence of the above derivations on the thermal noise in MOSFETs. Let's consider, for the sake of simplicity, the thermal noise in linear region where the MOSFET is a simple resistance. It can be easily extended to the nonlinear region by integration along the channel of the noise source using the Klaassen and Prins approach [20]. Nevertheless, in this case, according the Nyquist-Johnson relation, which derives from the most general fluctuation-dissipation theorem, the drain current thermal noise can be written as [21],

$$S_{Id} = 4.kT.\mu.\frac{W}{L}Q_i. \quad (15)$$

In an alternative approach, the thermal noise is related to the diffusion noise and can often be expressed as [6-8,21],

$$S_{Id} = 4.q.D.\frac{W}{L}Q_i. \quad (16)$$

In the case of Boltzmann's statistics, q.D=μ.kT (Eq. (2)), so that Eq. (16) well reduces to Eq. (15). However, in the case of metallic statistics, q.D=μ.E_f (Eq. (3)), *i.e.* also q.D=μ.Q_i/C_q, such that Eq. (16) becomes,

$$S_{Id} = 4.\mu.\frac{W}{L}\frac{Q_i^2}{C_q}. \quad \text{(wrong)} \quad (17)$$

This relation is obviously wrong since it would imply that the thermal noise in a metallic resistance would not follow the Nyquist-Johnson formula and would not cancel out at zero temperature. This

also means that Eq. (16) is not general and cannot handle the onset of degenerate statistics. Actually, this inconsistency comes from the fact that the total carrier number, Q_i/q, appearing in Eq. (16), is incorrectly used. As a matter of fact, in a metallic system, the carriers participating to the transport are located in the Fermi skin, which has an energy thickness of kT around the Fermi level E_f and are not equal to the total number of carriers in the band [22]. Indeed, according to the thermodynamic fluctuations, the carrier number in the Fermi skin is given by [22,23],

$$\Delta n = \int N(E).f.(1-f)dE = kT.\frac{\partial n}{\partial E_f}, \tag{18}$$

where f is the Fermi-Dirac function. Therefore, in a 2D subband inversion layer, the inversion charge in the Fermi skin now reads,

$$\Delta Q_i = kT.\frac{\partial Q_i}{\partial E_f} = \frac{kT}{q}.C_{inv}. \tag{19}$$

Replacing the total inversion charge Q_i by the inversion charge in the Fermi skin ΔQ_i in Eq. (16) allows to obtain the exact diffusion noise formula,

$$S_{Id} = 4.kT.D.\frac{W}{L}C_{inv}. \qquad \text{(exact)} \tag{20}$$

For further verification, we can check that, in the case of Boltzmann's statistics, $C_{inv} \approx q.Q_i/kT$, which means also that $\Delta Q_i \approx Q_i$, so that Eq. (20) well recovers Eq. (16), and by turn Eq. (15). Moreover, for metallic statistics, $C_{inv}=C_q$, and $q.D=\mu.E_f$ i.e. also $q.D=\mu.Q_i/C_q$, such that we check that Eq. (20) well reduces to Eq. (15). In the most general case, we have, from the generalized Einstein equation, $q.D=\mu.n.\partial E_f/\partial n$ i.e. also $D=\mu.Q_i/q.\partial E_f/\partial Q_i=\mu.Q_i.\partial \Psi_s/\partial Q_i=\mu.Q_i/C_{inv}$, so that Eq. (20) fully recovers Eq. (15).

Therefore, Eq. (20) does constitute the most general form of diffusion thermal noise in a MOSFET in ohmic regime. It can easily be extended to the nonlinear regime using the Klassen and Prins formula [20].

4. Results and discussion

Typical $I_d(V_g)$ characteristics for our template FDSOI device obtained using Eqs (10), (13) and (14) are shown in Fig. 4 for high and very low temperatures. At T=200K, as is well known, the diffusion current dominates at weak inversion, whereas the drift component prevails at strong inversion above threshold. At T=4K, the drift component also seems to prevail on diffusion above threshold, while the weak inversion region is squeezed out.

It should also be noted that, according to Eq. (14), the drift current is modulated by the partition capacitive ratio $C_{inv}/(C_{inv}+C_{ox})$, whereas the diffusion current is modulated by $C_{ox}/(C_{inv}+C_{ox})$. This means that the subthreshold slope of the diffusion current in weak inversion is the same as for the whole drain current since $C_{inv} \ll C_{ox}$, such that the partition capacitive ratio ≈1. Contrarily, for the drift

current, the partition capacitive ratio $\approx C_{inv}/C_{ox}$, and since C_{inv} is proportional to Q_i in weak inversion, the drift current varies as $I_d.Q_i$ i.e. also Q_i^2. As a result, the subthreshold slope of the drift current in weak inversion is equal to twice the subthreshold slope of the whole drain current. This feature well explains the subthreshold slope behavior in Fig. 4, better visible for T=200K, for the diffusion and drift current components.

In order to better visualize the diffusion and drift components, we have plotted in Fig. 5 the ratio between them and the drain current $R_{diff}=I_{ddiff}/I_d$ and $R_{drift}=I_{ddrift}/I_d$. As can be seen from this figure, at very low temperature, the diffusion current fully dominates below threshold, whereas the drift component totally vanishes. Above threshold, while using a constant mobility, the two components are almost flat and R_{diff} is equal here to $\approx$0.07 and R_{drift} to $\approx$0.93. These values correspond to the limit obtained using the diffusivity (Eq. (3)) and the inversion charge in Eqs (14) for degenerate metallic statistics. In fact, it is easy to show from Eqs (3) and (14) that these values are close to $C_{ox}/(C_{ox}+C_q)$ and $C_q/C_{ox}+C_q)$ since $C_{inv}\approx C_q$ in the degenerate case.

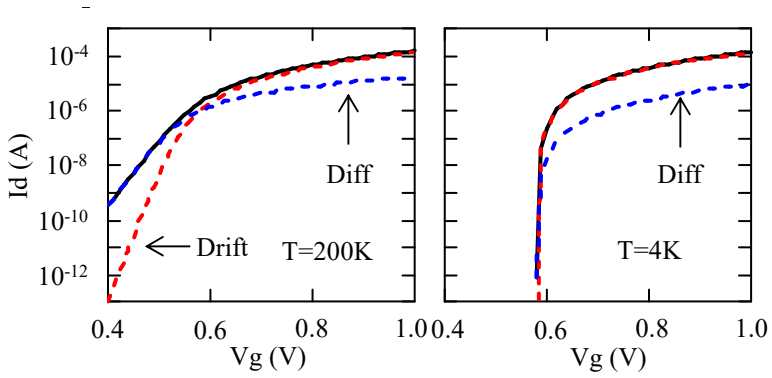

Fig. 4. $I_d(V_g)$ characteristics showing the drift and diffusion components for high and very low temperatures (constant mobility μ=1000cm^2/V$_s$, V_d=0.5V, V_b=0, W=L=1μm).

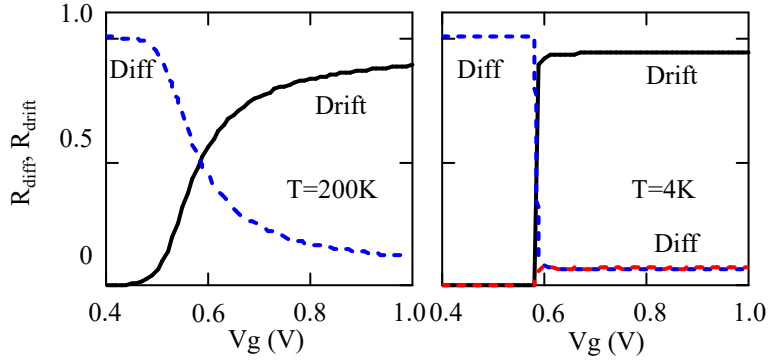

Fig. 5. $R_{diff}(V_g)$ and $R_{drift}(V_g)$ characteristics for high and very low temperatures. The red dashed line shows the $R_{diff}(V_g)$ for degenerate statistics for T=4K (constant mobility μ=1000cm^2/V$_s$, V_d=0.5V, V_b=0, W=L=1μm).

In Fig. 6a are also displayed the variations with drain voltage of the drain current along with the drift and diffusion components. In Fig. 6b are shown the corresponding $R_{diff}(V_d)$ and $R_{drift}(V_d)$ characteristics for two temperatures T=4K and T=200K. As can be seen, it should be noted that the ratios R_{diff} and R_{drift} are almost independent of drain voltage from linear to saturation region, especially for very low temperature.

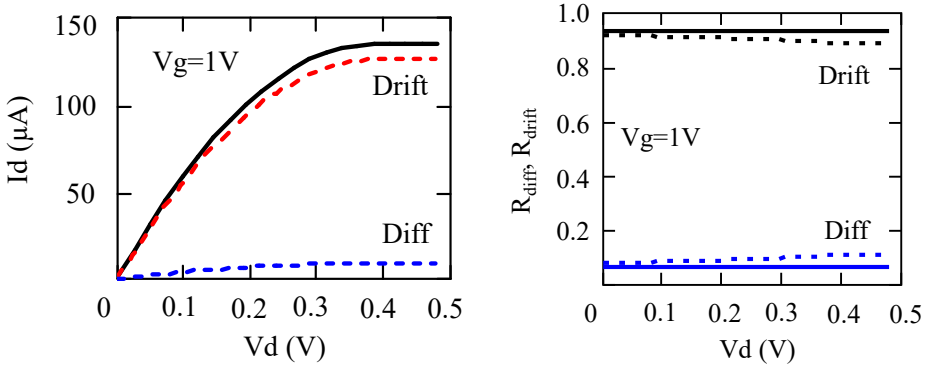

(a) (b)

Fig. 6. a) $I_d(V_d)$ characteristics at T=4K showing the drift and diffusion components. a) $R_{diff}(V_d)$ and $R_{drift}(V_d)$ characteristics for T=4K (solid lines) and T=200K (constant mobility μ=1000cm^2/V$_s$, V_d=0.5V, V_b=0, W=L=1μm).

Moreover, in Fig. 7 are displayed the temperature dependence of the diffusion and drift ratios, R_{diff} and R_{drift}, for two gate voltages, V_g=0.5V and V_g=1V, located in weak and strong inversion, respectively. As can be seen, the diffusion ratio R_{diff} depends slowly on temperature for both gate voltages. Instead, the drift ratio R_{drift} varies weakly with temperature in strong inversion (V_g=1V), whereas R_{drift} appears to be thermally activated in weak inversion below threshold (see Fig. 7c, V_g=0.5V).

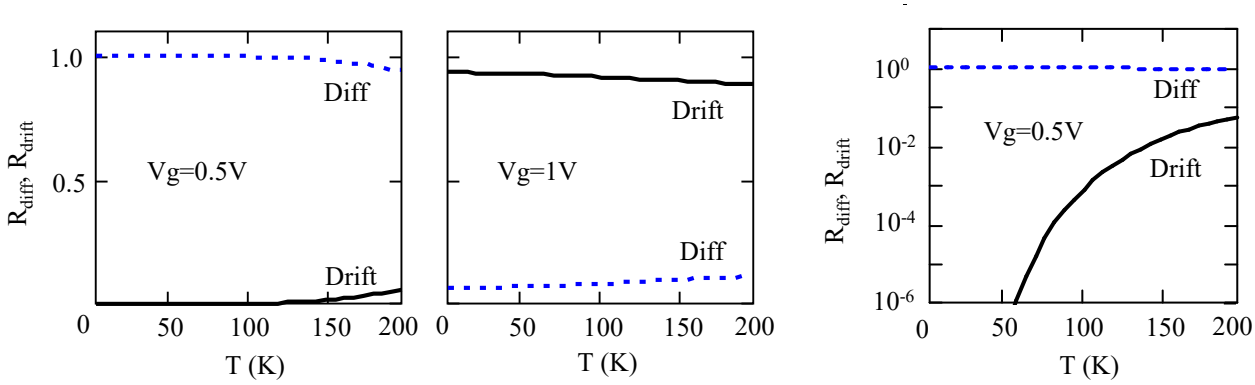

(a) (b) (c)

Fig. 7. a) and b) Variations with temperature of R_{diff} and R_{drift} for V_g=0.5V and V_g=1V in linear scale. c) Variations with temperature of R_{diff} and R_{drift} for V_g=0.5V in log scale (constant mobility μ=1000cm^2/V$_s$, V_d=0.5V, V_b=0, W=L=1μm).

The case of a non-constant mobility as those experimentally measured vs inversion layer density (see Fig. 3a) has been investigated for completeness purpose. To this end, we have introduced in the drain current equation (Eq. 10) an effective mobility depending of inversion charge Q_i with a bell-shaped form as observed at very low temperature [17]:

$$\mu_{eff} = \frac{2.\mu_m}{Q_i/Q_c + Q_c/Q_i} \tag{21}$$

where μ_m is the maximum mobility and Q_c a critical charge locating μ_m versus Q_i.

In Fig. 8 are compared the variation with gate voltage of the ratio $R_{diff}=I_{ddiff}/I_d$ as obtained with a non-constant mobility law (Eq. 21, black solid line), as well as for a constant mobility (triangle symbols). As can be seen from the figure, the curves are almost superimposed, indicating that the mobility law has no significant impact on the diffusion ratio R_{diff} and by turn on $R_{drift}=1-R_{diff}$. Moreover, as already discussed and suggested by Eq. (14b), the diffusion ratio mainly varies as the capacitance ratio $C_{ox}/(C_{ox}+C_{inv})$ (see red cross symbols in Fig. 8). The latter feature explains why the mobility law is not important factor in the diffusion vs drift partition scheme.

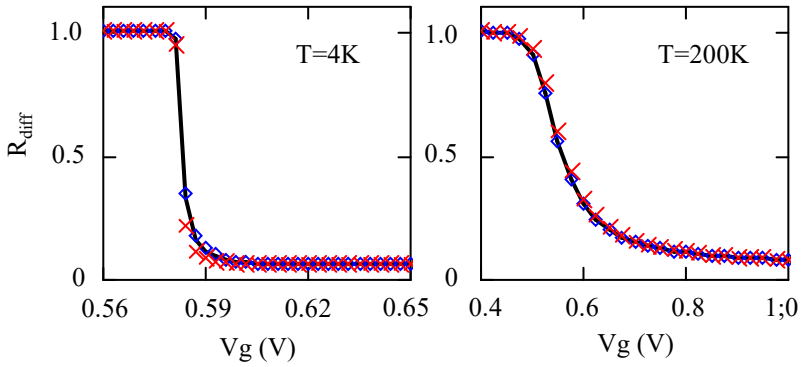

Fig. 8. $R_{diff}(V_g)$ characteristics for high and very low temperature: i) black dashed line for non-constant mobility of Eq. (21), ii) triangle symbols for constant mobility (μ=1000cm^2/Vs) and iii) red cross symbols for the ratio $C_{ox}/(C_{ox}+C_{inv})$ (μ_m=1000cm^2/Vs, Q_c=2.10^{12}q/cm^2, V_d=0.01V, V_b=0, W=L=1µm).

Finally, we illustrate in Fig. 9 the variations of the drain current thermal noise S_{Id} with gate voltage for two temperatures as obtained from various formulations. As can be seen, Eq. (20) provides exactly the same result as the Nyquist-Johnson formula (Eq. (15)) for both temperatures, emphasizing its validity. In contrast, Eq. (16) is only valid in weak inversion where the Boltzmann statistics applies, whereas it becomes incorrect at strong inversion, as much as the temperature is lowered, due to the onset of degenerate statistics.

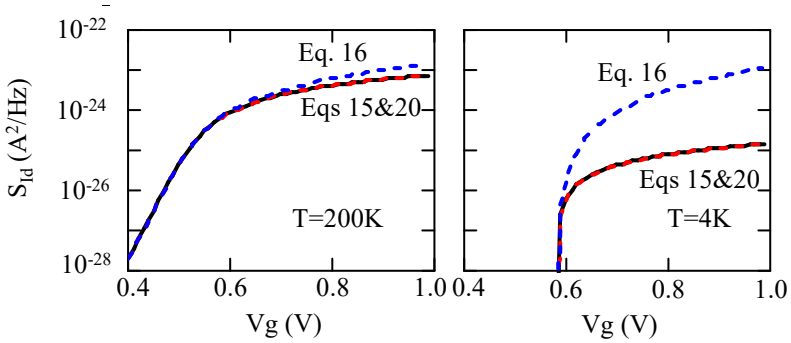

Fig. 9. Variations of drain current thermal noise S_{Id} with gate voltage V_g as obtained using different equations for T=200K and T=4K (constant mobility μ=1000cm^2/V$_s$, V_d=0.5V, V_b=0, W=L=1μm)

3. Summary and Conclusion

First, we have performed a detailed and didactic analysis of the diffusivity in a 2D inversion layer and shown its dependence on carrier density and temperature for Boltzmann, Fermi-Dirac and degenerate metallic statistics. Then, we have developed a comprehensive and original formulation of the diffusion and drift current components in a MOSFET. Their variation with gate voltage and drain voltage has been examined down to deep cryogenic temperature. In weak inversion, the subthreshold slope of the drift and diffusion components has been well interpreted by the partition capacitive ratio. In strong inversion, the diffusion current at T=4K has been found nearly constant whatever the mobility law. Finally, owing to our diffusivity analysis, we have proposed a new expression for the diffusion noise valid from weak to strong inversion down to very low temperature, perfectly compatible with the Nyquist-Johnson relation.

Acknowledgment: This work was partially supported by EU H2020 RIA project SEQUENCE under grant number 871764.

References

1. S.M. Sze and K.K. Ng, Physics of semiconductor devices (Wiley, Hoboken, NJ, 2007).
2. Y. Tsividis and C. Mc Andrew, Operation and modeling of the MOS transistor (Oxford Univ. Press New York, 2011).
3. J.M. Hornibrook, et al., Cryogenic control architecture for large-scale quantum computing, Phys. Rev. Applied, 3, 024010 (2015).
4. R. Maurand, X. Jehl, D. Kotekar-Patil, A. Corna, H. Bohuslavskyi, R. Lavieville, L. Hutin, S. Barraud, M. Vinet, M. Sanquer and S. De Franceschi, A CMOS silicon spin qubit, Nature Commun., 7, 13575 (2016).
5. A. Beckers, F. Jazaeri, H. Bohuslavskyi, L. Hutin, S. De Franceschi, and C. Enz, Characterization and modeling of 28-nm FDSOI CMOS technology down to cryogenic temperatures, Solid-State Electronics, 159, 106–115 (2019).
6. R. Sarpeshkar, T. Delbruck, C.A. Mead, White noise in transistors and resistors, IEEE Circuits and Devices Magazine, 9, 23-29 (1993).
7. M.S. Obrecht, E. Abou-Allam, T. Manku, Diffusion current and its effect on noise in submicron MOSFETs, IEEE Trans. On Electron Devices, 49, 524-526 (2002).
8. K. Han, H. Shin, K. Lee, Analytical drain thermal noise current model valid for deep submicron MOSFETs, IEEE Trans. on Electron Devices, 51, 261- 269 (2004).
9. N. W. Ashcroft and N. D. Mermin, Solid State Physics, (Holt, Rinehart and Winston, New York, 1988).
10. J.S. Dugdale, The electrical properties of metals and alloys (London, Arnold, 1977)
11. A.P. Gnädinger, and H.E.Talley, Quantum mechanical calculation of the carrier distribution and the thickness of the inversion layer of a MOS field-effect transistor, Solid-State Electronics, 13, 1301-1309 (1970).
12. G. Ghibaudo, Transport in the inversion layer of a MOS transistor: use of Kubo-Greenwood formalism, Journal of Physics C: Solid State Physics, 19, 767-780 (1986).
13. E. Arnold, Disorder-induced carrier localization in silicon surface inversion layers, Appl. Phys. Lett. 25, 705 (1974).
14. H. Bohuslavskyi, A. G. M. Jansen, S. Barraud, V. Barral, M. Cassé, L. Le Guevel, X. Jehl, L. Hutin, B. Bertrand, G. Billiot, G. Pillonnet, F. Arnaud, P. Galy, S. De Franceschi, M. Vinet, and M. Sanquer, Cryogenic Subthreshold Swing Saturation in FD-SOI MOSFETs described with Band Broadening, IEEE Electron Device Letters, 40, 784-787 (2019).
15. A. Beckers , F. Jazaeri , and C. Enz, Theoretical Limit of Low Temperature Subthreshold Swing in Field-Effect Transistors, IEEE Electron Device Letters, 41, 276-279 (2020).

16. G. Ghibaudo, M. Aouad, M. Casse, S. Martinie, F. Balestra, On the modelling of temperature dependence of subthreshold swing in MOSFETs down to cryogenic temperature, Solid-State Electronics, 170, 107820 (2020).
17. F. Balestra and G. Ghibaudo, Device and circuit cryogenic operation for low temperature electronics, Kluwer, Amsterdam (2001).
18. N. Planes et al., 28nm FDSOI technology platform for high-speed low-voltage digital applications, Symposium on VLSI Technology (VLSIT), 2012, pp. 133–134.
19. M. Aouad, S. Martinie, F. Triozon, T. Poiroux, M. Vinet, G. Ghibaudo, Poisson-Schrodinger simulation of inversion charge in FDSOI MOSFET down to 0K – Towards compact modeling for cryo CMOS application, Proc. EUROSOI-ULIS 2020, Caen, France, 2020.
20. F. M. Klaassen and J. Prins, Thermal noise in MOS-transistors, Philips Res. Reps., 22, 505-514 (1967).
21. A. Van der Ziel, Noise in Solid State Devices and Circuits (John Wiley & Sons, Inc., New York, 1986).
22. Ch. Kittel, Introduction to Solid State Physics (John Wiley and Sons, Inc. New York, 1976).
23. V. Palenskis, Drift mobility, diffusion coefficient of randomly moving charge carriers in metals and other materials with degenerated electron gas, World Journal of condensed matter Physics, 3, 73-81 (2013).